frontiers | Frontiers in Materials

TYPE Original Research
PUBLISHED 19 December 2024
DOI 10.3389/fmats.2024.1512374

OPEN ACCESS

EDITED BY
P. Davide Cozzoli,
University of Salento, Italy

REVIEWED BY
Jun Ren,
Yunnan University, China
Hartmut Fischer,
Netherlands Organisation for Applied Scientific Research, Netherlands

*CORRESPONDENCE
Wu Yao,
yaowuk@tongji.edu.cn

RECEIVED 16 October 2024
ACCEPTED 29 November 2024
PUBLISHED 19 December 2024

CITATION
Bian X, Yao W, Liao G, Liang G, She A and Wei Y (2024) Hydrophobic cement-based materials with micro-nano hierarchical structures: preparation, characterization, and stability assessment.
Front. Mater. 11:1512374.
doi: 10.3389/fmats.2024.1512374

Hydrophobic cement-based materials with micro-nano hierarchical structures: preparation, characterization, and stability assessment

Xiaolei Bian, Wu Yao*, Gang Liao, Guangwei Liang, Anming She and Yongqi Wei

Key Laboratory of Advanced Civil Engineering Materials of Ministry of Education, School of Materials Science and Engineering, Tongji University, Shanghai, China

With the increasing demand for durable and sustainable building materials, the development of superhydrophobic cement-based materials has gained significant attention. In this study, superhydrophobic cement-based materials with layered structures were fabricated. By replicating microstructures from sandpaper and applying nanoparticles and low-surface-energy materials, we achieved a water contact angle of 155.7°. The resulting material demonstrates excellent waterproof performance, low adhesion forces, and high resistance to damage, providing valuable insights for the development of durable, waterproof building materials for sustainable construction.

KEYWORDS

micro-nano hierarchical structures, polydimethylsiloxane, hydrophobic, surface roughness, cement

1 Introduction

Cement-based materials are a kind of fundamental building material and they have been extensively utilized in various kinds of construction projects (Zhang W. et al., 2020; Wu et al., 2022). They have the benefits of easy construction, good durability, material savings, and low overall cost (Xu et al., 2022). These materials are widely employed in the construction of various engineering structures, such as residential buildings (Meng et al., 2023), bridges (Palacios et al., 2022) and roads (Li et al., 2022). However, due to the hydrophilic nature and inherent porosity of cement-based materials, they are susceptible to various physical and chemical reactions throughout their service life. These reactions ultimately lead to the formation of cracks, corrosion, and other defects in the cement matrix. As a result, structural damage and reduced durability of the cement-based materials occur (Nguyen et al., 2020; Wang et al., 2022). Generally, the durability of cementitious materials is closely related to the amount of water molecules that enter the material through the pores (Zhao et al., 2022). Therefore, controlling the amount of water molecules that penetrate the material is the most effective way to improve the durability and service life of cementitious materials.

Hydrophobic modification is an essential method to control the penetration of water molecules into materials. By changing the chemical structure, surface energy, and morphology of the material surface, the affinity between the material and water can be reduced, and the infiltration and adsorption of water molecules can be prevented. This

modification method is widely used in various fields, such as construction materials, textiles, electronic devices, *etc.* The durability, corrosion resistance, and performance stability of the material can be improved. So far, various methods that aim to fabricate robust superhydrophobic surfaces have been developed, such as templating (Tonon et al., 2023), etching (Lan et al., 2023), self-assembly (Shi et al., 2023), chemical vapor deposition (Su et al., 2023), electrospinning (Chen H. et al., 2023), and sol-gel (Wang et al., 2023). Moreover, these methods have been applied to create superhydrophobic surfaces on different substrates, such as metals (Zhao et al., 2023), ceramics (Zhang et al., 2023), polymers (Chen K. et al., 2023), and concrete (Wu Y. et al., 2023). Nevertheless, due to the specificity of cement-based materials that stem from their hydrophilicity and porosity, most of these methods are not suitable for preparing robust superhydrophobic cement-based materials. Currently, only a few methods can be used for the preparation of superhydrophobic cement-based materials, such as internal mixing (Wu F. et al., 2023), templating (Liu et al., 2017), external coating (Wang F. et al., 2021; Wu Y. et al., 2023), and so on. These methods, namely integral hydrophobic modification and surface hydrophobic modification, mainly represent two directions in hydrophobic modification of cement-based materials at home and abroad (Muzenski et al., 2020; Wang W. et al., 2020; Liang et al., 2023). Integral hydrophobic modification involves mixing hydrophobic materials or modifiers into cement-based materials to achieve integral modification of cement-based structures. The resulting hydrophobic cement-based materials still retain their internal hydrophobic properties. However, some studies have shown that the strength of cement-based materials may be reduced after modification with hydrophobic mixtures (She et al., 2020; Li et al., 2021; Yu et al., 2021). And a trade-off and optimization between hydrophobic performance and strength is required. Surface hydrophobic modification involves the preparation of cement-based materials with special structures on the surface or the application of hydrophobic suspensions, organic solutions, or emulsions containing micro/nanoparticles on the surface of cement-based materials to achieve surface modification. Compared to integral modification, surface modification requires only treating the surface of cement-based materials without changing the formulation and performance of the whole material, which can effectively save costs. The overall performance of the resulting cement-based materials is less affected, and the mechanical properties of the original materials can be retained (Gao et al., 2019; Wang N. et al., 2021).

The hydrophobic coating on the surface of surface-modified cement-based materials, as well as the prepared microstructures, are frequently subjected to mechanical damage, including friction and collision. This is a significant factor influencing the hydrophobic stability of hydrophobic cement-based materials. Besides mechanical damage, hydrophobically modified cement-based materials must also resist acid and alkali corrosion (Sow et al., 2021). Silane-based hydrophobic materials are susceptible to corrosion by acids and alkalis. In alkaline environments, the majority of silane-based materials undergo hydrolysis, resulting in the breakage of silicon bonds and the detachment of hydrophobic groups. This leads to a reduction in hydrophobicity (Indumathy et al., 2023). Moreover, the stability of hydrophobic organic coatings is susceptible to deterioration when exposed to elevated temperatures and ultraviolet (UV) radiation (Zhao et al., 2022). Elevated external temperatures increase molecular thermal motion, causing degradation and cross-linking of certain polymers (Szafarska et al., 2023). When temperatures exceed a critical point, the coating material may undergo a phase transition. This can result in the loss of its hydrophobic properties or the breakdown of its rough structures. Therefore, investigating the stability of hydrophobic surfaces is essential. Mechanical damage is typically demonstrated through sandpaper abrasion, knife scratching, tape peeling, simulated rain impact, and wind-sand abrasion tests. Han et al. (2024) found that their superhydrophobic coating maintained a contact angle greater than 140° even after multiple peeling and abrasion cycles, retaining its hydrophobicity. Acid and alkali corrosion damage is mainly tested through acid and alkali immersion. Ni et al. (2021) immersed their eco-friendly, intelligent self-healing coating samples in salt solution, strong acid solution, and strong alkali solution. The effects of high temperature and UV radiation on hydrophobic organic coatings are mainly verified through temperature cycling tests and UV exposure. Cao et al. (2024) evaluated the outdoor durability of superhydrophobic coatings through simulated rain tests, wind-sand abrasion tests, and UV exposure tests. Jiang et al. (2023) conducted temperature cycling tests on negative carbon superhydrophobic self-cleaning concrete coatings.

At present, A lot of work has focused on preparing hydrophobic cement-based materials by simply replicating structures with hydrophobic properties, such as lotus leaf surfaces (Liu et al., 2017). However, the exploration of control parameters for surface roughness structure is not clear. In this study, a templating method was used to replicate the working surface of sandpaper and prepare cement-based materials with a micrometer structure. Then, polydimethylsiloxane (PDMS) and hydrophobic nano-silica (nano-SiO_2) were mechanically mixed and sprayed onto the surface of cement-based materials with micrometer structure to fabricate hydrophobic cement-based materials with micro-nano hierarchical structure. By varying the mesh size of sandpaper and the amount of nano-SiO_2, different micro-nano hierarchical structures can be fabricated. These structures can regulate the hydrophobicity and capillary water absorption of hydrophobic cement-based materials. At the same time, based on the fractal theory, the surface structure was reconstructed in three dimensions. The key control parameters of surface roughness were proposed, and the relationship between the surface structure and wettability of cement-based materials was quantitatively evaluated. Meanwhile, the performance of the prepared hydrophobic cement-based materials was also evaluated.

2 Experimental procedure

2.1 Materials

The Portland cement (P.O 42.5) employed in the present study was obtained from the China Tianrui Group Cement Co. Ltd. The nano-SiO_2 (particle size 7–40 nm, specific surface area 115 m^2/g) was supplied by Aladdin Biochemical Technology Co., Ltd. (Shanghai, China). The PDMS (DOWSIL 184) and the curing agent (SYLGARD 184) were sourced from Dow Corning Corporation, United States. The chemical composition of the curing agent was determined to be octamethylcyclotetrasiloxane. PDMS was observed to have a high viscosity and to be difficult to

process, and thus a non-polar organic solvent, n-hexane, was added to dilute the PDMS. The n-hexane was sourced from Shanghai Titan Technology Co., Ltd. All chemical reagents were utilized in their original form, with no subsequent purification. Sandpaper (120–2000 grit) was purchased from Guangdong Ruite Technology Co., Ltd. All experiments were carried out using deionized water.

2.2 The fabrication of micron-structured surfaces

Using sandpaper as a template, cement-based materials with micron-structured surfaces were prepared by silicone rubber molding method. In brief, silicone rubber molds ($35 \times 35 \times 35$ mm^3) were prepared by using sandpaper with different grit numbers as templates and mixing silicone rubber and curing agent at a ratio of 1:1. Ordinary Portland cement and deionized water were mixed at a water-to-cement ratio of 0.35 to prepare cement paste, which was stirred for 5 min to ensure sufficient mixing. Then the cement paste was cast and vibrated in the molds. After 24 h, the samples were de-molded to obtain cement-based materials with micron-structured surfaces. Next, PDMS, curing agent, and n-hexane were mixed at a mass ratio of 1:0.1:5 and stirred thoroughly. And then sprayed on the surface of cement-based materials to reduce their surface energy.

2.3 The fabrication of nanostructured surfaces

PDMS, curing agent, and n-hexane were mixed at a mass ratio of 1:0.1:5 and stirred thoroughly, and then a certain amount of hydrophobic nano-SiO_2 was added and stirred continuously for 5 min. The prepared composite was sprayed on the surface of cement-based materials with micron-structured surfaces using an electric spray gun. The sprayed cement-based materials were cured in an oven at 40°C for 24 h to obtain cement-based materials with hierarchical micro-nano structures. However, it is worth noting that in practical applications, the curing temperature is lower than 50°C, so the curing process will take longer. And the curing temperature only affects the curing time, not the performance. The mass ratios of nano-SiO_2 to PDMS were 0.02, 0.04, 0.06, 0.08, and 0.1, respectively. As a control sample, a pure PDMS coating was prepared.

2.4 Characterization

The surface morphology and microstructure of hydrophobic cement-based materials were observed by optical microscope (GP-680, GAOPIN, China). The functional groups of hydrophobic cement-based materials were characterized by Fourier transform infrared spectrometer (EQUINOX 55, Bruker, Germany) using the attenuated total reflection (ATR) method, and the Fourier transform infrared spectra (FTIR) were drawn. We calculated the three-dimensional surface fractal dimension of the hydrophobic surface based on the optical microscope images. The specific calculation process included the following steps: (1) Determine the region of interest of the optical image, and convert the target image into a grayscale image, extracting the grayscale values of each pixel; (2) Reconstruct the three-dimensional surface profile using the grayscale values as height values; (3) Apply the Minkowski–Bouligand dimension method to calculate the fractal dimension from the grayscale image, as shown in Equation 1 (Liao et al., 2023b):

$$D = \lim_{n\to\infty} \frac{\ln N_n(A)}{\ln 2^n} \tag{1}$$

where D is the surface fractal dimension. A is the target area. $1/2^n$ is the length of the cubic box. And $N_n(A)$ is the minimum number of cubic boxes required to cover the target area. By performing linear regression analysis on $\ln 2^n$ and $\ln N_n(A)$, the regression coefficient obtained is the fractal dimension. The wettability of hydrophobic cement-based materials was characterized by water contact angle (WCA), which was measured by a contact angle meter (DSA25, Kruss, Germany). The test liquid was 2 μL deionized water. The WCA was tested at five different positions on the sample surface, and the average value of each position was used for WCA analysis.

2.5 Water absorption measurement

The water absorption performance of hydrophobic cement-based materials was evaluated with reference to the German standard DIN 52617–1987. Three cubic samples ($35 \times 35 \times 35$ mm^3) were used for the water absorption measurement. Before the measurement, the sample was dried at 60°C for 48 h until constant weight. Then, the side faces of each cubic sample were sealed with paraffin wax. The samples were placed in water, with the hydrophobic surface horizontally immersed 2–3 mm below the water level. The bottom of the sample was supported by a ϕ 10 steel bar to ensure the water absorption area of the sample. The water absorption rate of the sample was determined by measuring the weight of the sample after different immersion times. Then, the capillary water absorption coefficient of the sample was calculated by the following Equations 2, 3:

$$A = \delta/\sqrt{t} \tag{2}$$

$$\delta = (w_t - w_0)/S \tag{3}$$

where A is the water absorption coefficient, δ is the water absorption per unit area of the specimen (kg/m^2), t is the immersion time (min), w_t is the weight of the specimen at time t (kg), w_0 is the weight of the specimen before the experiment (kg), and S is the area of the hydrophobic surface of the specimen (m^2).

3 Results and discussion

3.1 Analysis of surface microstructure

It is widely acknowledged that the microstructure and chemical composition of a solid surface are pivotal in determining its wettability (Wang et al., 2020a; Wu Y. et al., 2023; Heo et al., 2024; Tao et al., 2024). Therefore, the microstructures of the hydrophobic surfaces of all samples prepared using sandpaper with grit sizes of 120, 220, 400, 800, 1,200, and 2000, respectively were tested,

and the results are shown in Figure 1. As shown in the figure, the surfaces of all samples are rough and similar to the sandpaper structure, indicating that the microstructure of the sandpaper was successfully transferred to the cement-based material surface. In addition, a multitude of pores can be observed when the grit size is below 800, with the pore size being directly proportional to the sandpaper's grit. It is evident from the figures that, before a grit size of 800, the size of the surface protrusions and pores decreases as the sandpaper's grit increases. The complexity of the sample surface, facilitated by the synergy between the surface protrusions and pores, continuously escalates. Consequently, it is distinctly noticeable that during the transition from 120 to 400 grit, the surface roughness of the sample progressively increases. After the grit size exceeded 800, the shape and size of the surface particles became similar, and the comparison of the surface roughness was no longer clear. Considering that the hydrophobic performance is closely related to the surface roughness of the material, generally speaking, the higher the hydrophobic surface roughness, the better the hydrophobic performance (Mao et al., 2020). According to the Wenzel model and the Cassie–Baxter model, when the contact angle of the ideal smooth surface is greater than 90°, the increase of the surface roughness factor and the liquid-solid contact area ratio will increase the apparent contact angle, that is, the hydrophobic performance is enhanced (Wenzel, 1936; Cassie and Baxter, 1944). This phenomenon occurs because as surface roughness increases, the actual surface area of the material also expands. However, at the same time, water droplets remain suspended on the protrusions of the rough surface, resulting in a reduced actual contact area between the water droplets and the material surface. Since the surface roughness of the hydrophobic surface of the sample affects the effect of solid-liquid contact, the accurate measurement of the surface roughness of the sample is of great significance for the prediction of the hydrophobic performance. The roughness is the ratio of the actual solid face to the projected solid face. It is difficult to quantify the actual solid face, so only some qualitative measures are available to describe the roughness (Lange et al., 1993; Packham, 2003). To solve this problem, we propose a new definition of surface roughness, as shown in Equation 4 (Liao et al., 2023a):

$$r = D_r/D \tag{4}$$

where r is the surface roughness, D_r is the fractal dimension of the sample surface, and D is the fractal dimension of the smooth surface, which is 2. This equation allows for the straightforward calculation of the surface roughness of various samples. The calculations demonstrate that the surface roughness increases markedly with particle size between 120 and 400, reaching a high level of 1.2372 at 400 grits and rapidly approaching the theoretical maximum roughness value of 1.5. This result is consistent with our previous analysis. Beyond a grit size of 800, the roughness remains relatively unchanged, stabilizing around 1.2372. This phenomenon may be attributed to the fact that, compared to small grits, the larger grit sandpaper produces more protrusions on the sample surface, but the integrity of these protrusions is compromised, resulting in a lower longitudinal height than those prepared with finer grit sandpaper. Additionally, the larger grit sandpaper results in fewer surface pores, diminishing the synergistic effect of the pores and affecting the overall complexity of the surface. Given that the roughness at 400 grits has reached a considerably high level and further increases in grit size do not result in significant changes in roughness, it can be inferred that at 400 grits, the microscale contribution to roughness has achieved a relatively high level.

3.2 Wettability

To investigate the influence of different grit sizes of sandpaper used as templates on hydrophobic properties, Figures 2A–F shows the WCAs of the cement-based materials prepared with various grits of sandpaper and coated with PDMS. The corresponding WCA measurements are shown in Figure 3. The result indicates that the WCAs of the hydrophobic surfaces of cementitious materials prepared with 120, 220, and 400 grits of sandpaper gradually increase, stabilizing after 400 grits. The prepared samples exhibit WCAs ranging between 136.6° and 146.0°. On these surfaces, water droplets transition from ellipsoidal to perfectly spherical shapes. Additionally, the WCAs correlate highly with the surface roughness analyzed earlier. Before 400 grit, as the roughness rapidly increases, so does the WCA. Beyond 400 grit, the roughness values maintain around 1.2372, and the WCAs remain approximately constant near 145.5°. Based on the wetting behavior of water droplets on the samples, the wetting model of the hydrophobic cement-based materials prepared using sandpaper aligns more closely with the Wenzel model. According to the Wenzel model, as shown in Equation 5 (Wenzel, 1936):

$$\cos\theta_\gamma = \gamma(\gamma_{SG} - \gamma_{SL})/\gamma_{LG} = \gamma\cos\theta \tag{5}$$

where θ_γ is the apparent contact angle in the Wenzel model, θ is the intrinsic contact angle, and γ is the roughness factor of the solid surface, which is the ratio of the actual solid-liquid interface contact area to the projected contact area. In the Wenzel model, an increase in the roughness of the solid surface results in a corresponding increase in the degree of wetting (Chen Z. et al., 2023). This implies that a rougher hydrophilic surface will demonstrate increased hydrophilia, whereas a rougher hydrophobic surface will display enhanced hydrophobic properties. Before 400 grit, as the grit size of the sandpaper increases, the surface roughness of the prepared cementitious material also increases, enhancing the complexity of the material's surface with raised features and pores. Due to material consistency, the surface free energy of the material reaches its lowest after 400 grit. The higher the surface free energy, the weaker the hydrophobicity; the lower the surface free energy, the stronger the hydrophobicity. The enhancement of the material's hydrophobic properties is evident, hence the hydrophobic cementitious materials prepared with 400-grit sandpaper demonstrate superior hydrophobic performance compared to those prepared with 120-grit and 220-grit sandpaper. When the particle size reaches beyond 800, there is a negligible change in roughness and the WCA, due to the surface complexity being relatively stable. This stability is influenced by an increase in the number of surface protrusions, a reduction in surface completeness, and a decrease in surface porosity. At this stage, it is challenging to further increase the roughness of the micro-scale structures. The microstructures on the surface cause droplets to assume a nearly spherical shape, causing the WCA to approach a

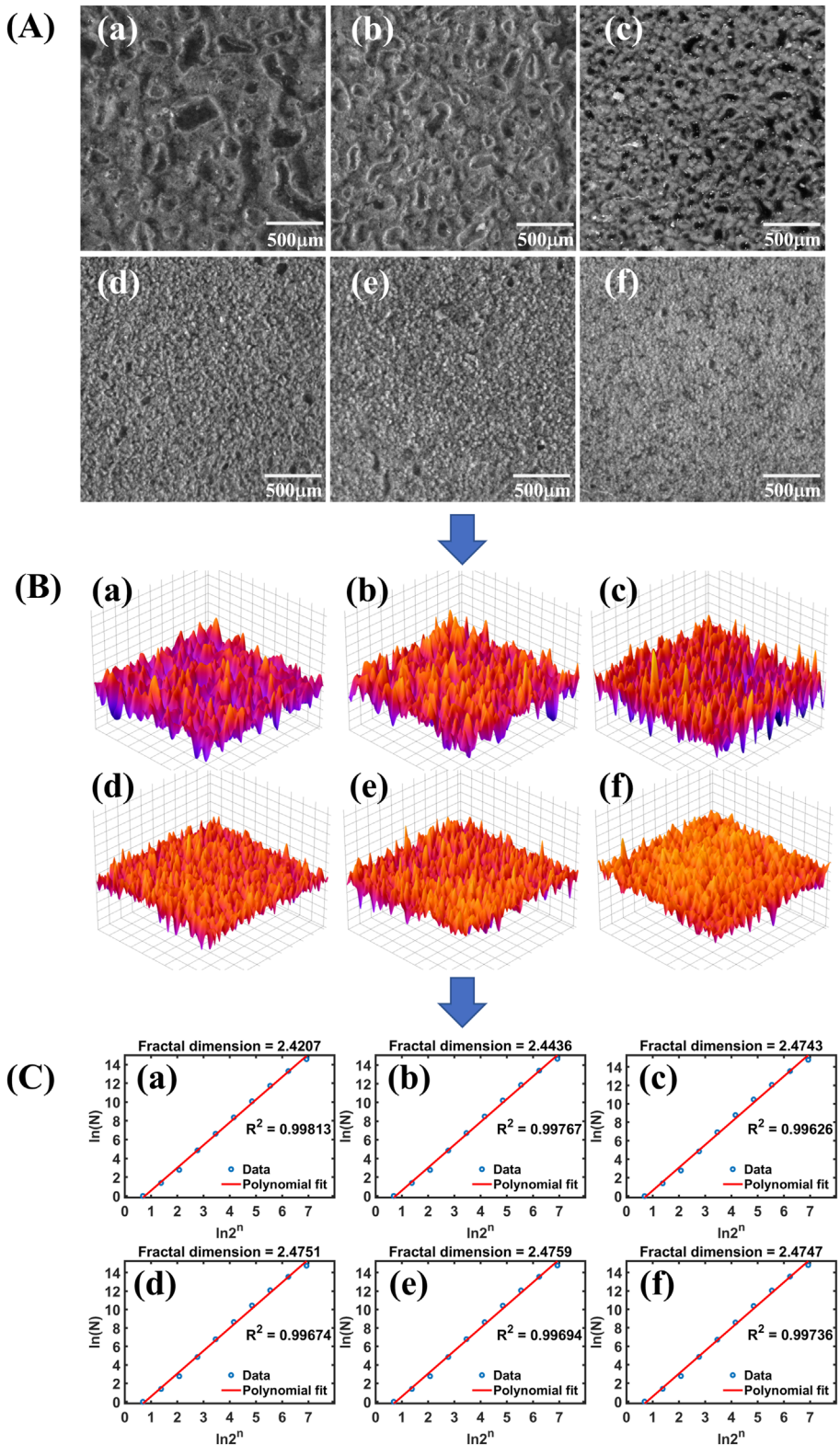

FIGURE 1
Optical images and surface fractal dimensions of hydrophobic surfaces prepared with different sandpapers for hydrophobic cement-based materials. **(A)** Optical images: **(a-f)**: 120-grit, 220-grit, 400-grit, 800-grit, 1200-grit, 2000-grit; **(B)** Three-dimensional reconstruction maps: **(a-f)**: 120-grit, 220-grit, 400-grit, 800-grit, 1200-grit, 2000-grit; **(C)** Fractal dimensional fitting maps: **(a-f)**: 120-grit, 220-grit, 400-grit, 800-grit, 1200-grit, 2000-grit.

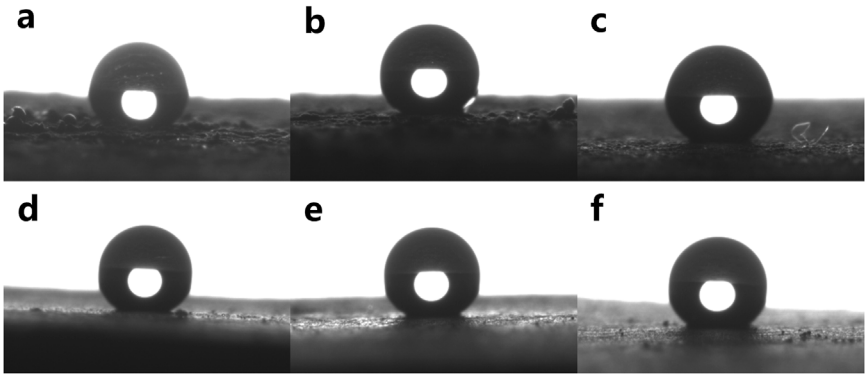

FIGURE 2
Wetting states of hydrophobic cement-based materials prepared with different sandpaper grit sizes in contact with water droplets: **(A)** 120-grit; **(B)** 220-grit; **(C)** 400-grit; **(D)** 800-grit; **(E)** 1200-grit; **(F)** 2000-grit.

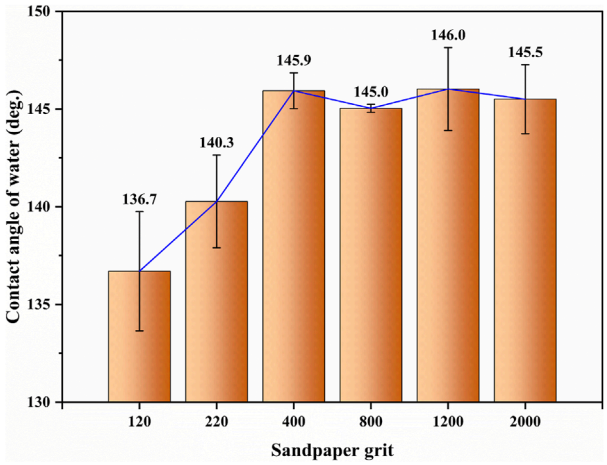

FIGURE 3
Effect of different sandpaper grit sizes on the hydrophobicity of the sample surface.

maximum value, consistent with the Wenzel model. Consequently, with higher grit sandpapers, the impact of increased micro-roughness on WCA tends to saturate, maintaining the WCA at a stable level. Meanwhile, 400 grit sandpaper provides moderate micro-pores and protrusions, which contribute to the formation of a stable hydrophobic layer due to the uniformity of the structure. At higher grit sandpaper, the microstructure becomes finer, resulting in a non-significant increase in the overall structural complexity of the surface and thus little change in WCA. As described, the surface roughness parameter significantly reveals the hydrophobic mysteries of various sample surfaces. This key parameter is an essential tool for the conceptualization and design of sample surfaces, aiding in the precise design of surface roughness to meet specific hydrophobicity standards.

To investigate the effect of different doping amounts of nanoparticles on the hydrophobic performance, the additional amount of nano-SiO_2 was varied. The surface hydrophobic performance is shown in Figure 4, and the measurement values are shown in Figure 5. As can be seen from the figure, the WCA of the pure PDMS hydrophobic cement-based material surface without adding nanoparticles is 145.9°. This is due to the low intrinsic surface energy of PDMS (Tang et al., 2023) and the significant contribution of the 400-grit sandpaper structure to the micron-scale structure. However, there is a limit to the enhancement of the surface contact angle by constructing only the micron-scale structure. When the sandpaper particle size reaches 400 grit, the improvement of the hydrophobic performance by the micron-scale structure has reached the limit. According to the binary synergistic theory of Jiang (2003), the nanostructure plays an important role in the construction of superhydrophobic surfaces with high contact angles. At this time, smaller nanoparticles are needed to composite with the micron-scale structure to form a micro-nano hierarchical structure. After doping with nanoparticles, nano-SiO_2, and micron-scale protrusions together form a multi-scale micro-nano gas-solid composite surface structure, which is in good agreement with the contact angle model of the composite surface proposed by Cassie–Baxter.

The effect of nano-SiO_2 content on the WCA of the hydrophobic surface is shown in Figures 6, 7. The results demonstrate a tendency for the hydrophobicity of hydrophobic cement-based materials to increase and subsequently decline as the concentration of nanoparticles rises. When the nano-SiO_2 content is less than 4wt%, the WCA increases rapidly from 145.9° to the maximum value of 155.7°, indicating the enhancement of the hydrophobicity of the hydrophobic cement-based materials. When the nano-SiO_2 content is further increased, the WCA slightly decreases, but remains above 150°, maintaining superhydrophobic performance. When the nano-SiO_2 content is increased to 10wt%, the WCA drops rapidly below 150°. The change in the WCA is mainly attributed to the surface microstructure of the hydrophobic cement-based materials. According to the Cassie–Baxter model, as shown in Equation 6 (Cassie and Baxter, 1944):

$$\cos\theta_y = f_1 \cos\theta_1 + f_2 \cos\theta_2 \tag{6}$$

where θ_y is the apparent contact angle in the Cassie–Baxter model, θ_1 is the intrinsic contact angle of the liquid on the solid-liquid

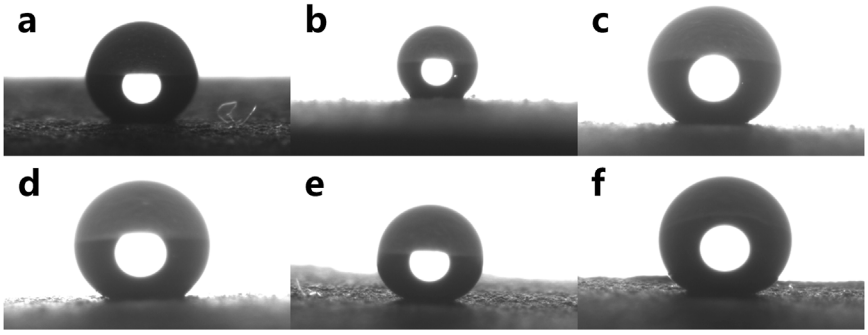

FIGURE 4
Wetting states of hydrophobic cement-based materials prepared by spraying PDMS with different nano-SiO_2 contents: **(A)** 0 wt.%; **(B)** 2 wt.%; **(C)** 4 wt.%; **(D)** 6 wt.%; **(E)** 8 wt.%; **(F)** 10 wt.%.

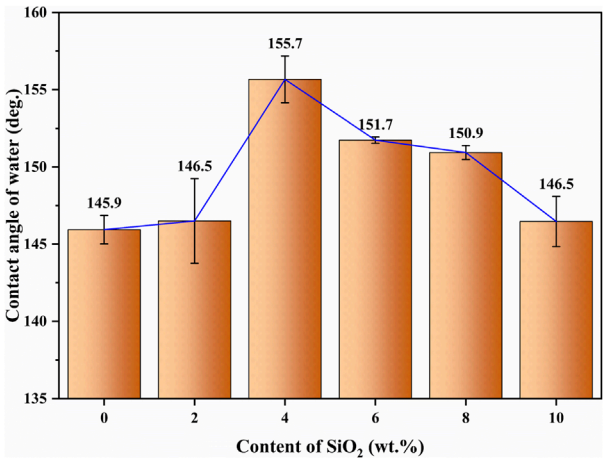

FIGURE 5
Effect of PDMS with different nano-SiO_2 contents on the surface hydrophobicity of samples.

interface, θ_2 is the intrinsic contact angle of the liquid on the liquid-gas interface, f_1 is the fraction of the solid-liquid contact area on the rough surface, f_2 is the fraction of the liquid-gas contact area on the rough surface, and $f_1 + f_2 = 1$. The rough surface has two types of contact areas: solid-liquid and liquid-gas. The volume of air trapped between the solid surface and the droplet depends on the fraction of these contact areas. If the fraction of the solid-liquid contact area is reduced or the fraction of the liquid-gas contact area is increased, the trapped air volume will increase. This will form larger air pockets that support the droplet on the rough surface (Wang et al., 2015). As a result, the WCA will also increase. The nano-SiO_2 content significantly influences the surface structure of hydrophobic cement-based materials. At lower nano-SiO_2 contents (below 4 wt%), nano-SiO_2 particles preferentially fill the grooves of the replicated sandpaper structure, resulting in an insufficient number of nanoparticles adhering to the surface protrusions (Xia and Brueck, 2008). In this scenario, most nano-SiO_2 particles are concealed beneath the PDMS layer, with only a few exposed on the surface (Yu et al., 2022). The surface structure exhibits a combination of large-scale smoothness and small-scale roughness, primarily reflecting the inherent characteristics of PDMS and the micrometer-scale structure formed by 400-grit sandpaper. Consequently, a minor nano-SiO_2 content does not significantly enhance the hydrophobicity of the cement-based materials, with the surface contact angle being comparable to that of the 400-grit hydrophobic cement-based material solely coated with PDMS. As the nano-SiO_2 content increases, more particles are exposed on the PDMS surface. At a 4 wt% nano-SiO_2 content, nano-SiO_2 can be evenly distributed on the sample surface, forming a micro-nano hierarchical structure consistent with the Cassie–Baxter model, thereby markedly enhancing the geometric morphology and surface roughness complexity of the hydrophobic cement-based materials. At this content, the nanostructures formed by nano-silica create additional air pockets between themselves and the micrometer structures formed by 400-grit sandpaper, preventing direct contact between droplets and the micrometer-scale structures. This reduces the solid-liquid contact area on the rough surface, resulting in a larger WCA of 155.7°. It is noteworthy that at higher nano-SiO_2 contents, the sample surface exhibits a multitude of unevenly sized particles. These larger particles may form due to the aggregation of nano-SiO_2 in the PDMS solution (Ammar et al., 2017). With an increase in nano-SiO_2 content, the presence of large-scale particles on the sample surface gradually increases due to the heightened likelihood of aggregation. These clusters may mask or fill the microscopic rough structure, thus affecting the micro- and nano-hierarchical structure of the surface and leading to a decrease in the water contact angle (Zhang X.-F. et al., 2020). These effects are detrimental to the control of the micro-nano hierarchical structures discussed in this paper. When the nano-SiO_2 content exceeds 10 wt%, there is a noticeable decline in the WCA. This is likely due to the 30-micrometer diameter of the spray gun nozzle used in this study. At a nano-SiO_2 content of 10 wt%, the nanoparticles tend to aggregate into larger particles, leading to the clogging of the nozzle. This aggregation makes it difficult for the nanoparticles to be uniformly distributed with PDMS on the sample surface. Additionally, when the particle size reaches the nozzle diameter, it implies that the nanoparticles have reached the micrometer scale, making it challenging to contribute to the nanostructure.

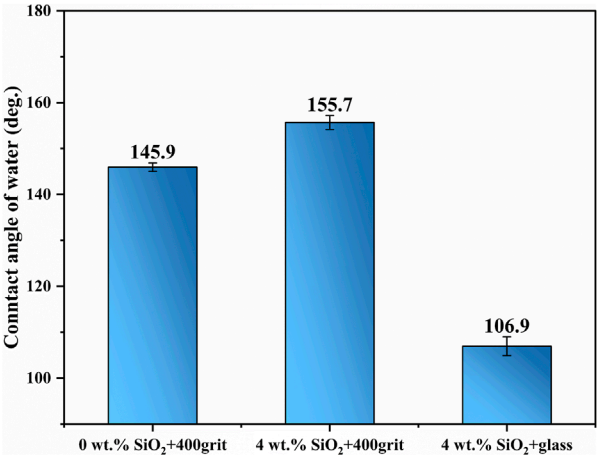

FIGURE 6
Surface contact angle of samples with different spraying substances and different substrates.

Figure 6 shows the surface wetting states of 400-grit cement-based material sprayed with PDMS, 400-grit cement-based material sprayed with PDMS containing 4 wt% nano-SiO_2, and glass sprayed with PDMS containing 4 wt% nano-SiO_2, respectively. As shown in the figure, the contact angle of the material prepared by coating PDMS with 4 wt% nano-SiO_2 on glass is only 106.9°, while the contact angle of the material prepared by coating PDMS with 4 wt% nano-SiO_2 on 400-mesh cement-based materials can be increased to 155.7°. This indicates that the micron structure prepared in this paper by replicating the surface structure of sandpaper has a promising enhancement effect in the contact angle range of 100°–145° interval. Compared with the material prepared by coating PDMS with 4 wt% nano-SiO_2 on 400-mesh cement-based materials, the contact angle of the material prepared by only coating PDMS on 400-mesh cement-based materials is 145.9°. This suggests that micron structures prepared by simply replicating the surface of sandpaper have an upper limit on the enhancement of the contact angle of the material. Before reaching the upper limit, the micron structure can have a greater impact on the wetting property of the material surface. After reaching the upper limit, the improvement of the contact angle needs the help of a new nanostructure. The nanostructure prepared by this paper can continue to increase the contact angle of the material after the micron structure reaches the upper limit (Zhu and Duan, 2024). So that it reaches a contact angle of 150° or more, which is what superhydrophobic materials have.

3.3 Adhesion to water

Figure 7 shows the bouncing behavior of the samples with 2 wt%, 4 wt%, and 6 wt% of nano-SiO_2. No bouncing behavior of water droplet on the sample surface occurred on the sample surface when the nano-SiO_2 content was 2 wt% and 6 wt%, while the water droplet bounced twice on the sample surface when the nano-SiO_2 content was 4 wt%. This demonstrates the high adhesion force on the surface of the sample block at 2 wt% nano-SiO_2, although hydrophobicity was achieved (Schutzius et al., 2015). This is because the nano-SiO_2 content was low at this point, and the nano-SiO_2 particles were sparsely distributed on the micrometer structure surface. These nano-SiO_2 particles were too dispersed to support the water droplet. The water droplet completely entered the groove structure of the solid rough surface and contacted the solid surface closely, which was consistent with the Wenzel model (Shen et al., 2021; Yu et al., 2022). Therefore, it can be considered that the sample was in the Wenzel state at this point. At 4 wt%, the number of nanoparticles was optimal. These nanoparticles could be distributed uniformly on the sample surface, forming a micro-nano hierarchical structure with the micron structure obtained by replicating the working surface of the sandpaper (He et al., 2024). At this point, the uneven solid surface did not wet completely when contacting the liquid. The droplet only approached the solid surface infinitely but never touched the groove surface. The gas in the rough surface layer replaced part of the solid and liquid contact, which was consistent with the Cassie–Baxter model. Therefore, it can be considered that the sample was in the Cassie state at this point. At 6 wt%, the amount of nano-SiO_2 was large, and aggregation occurred on the sample surface. Some nanostructures were covered, and the remaining nanostructures increased the contact angle of the sample surface but did not have a significant effect on the bouncing behavior (Ammar et al., 2017; Zhang X. F. et al., 2020). Similar to the 2 wt% content, no bouncing of water droplets occurred on the sample surface. However, considering that the contact angle was increased at this point, it can be considered that the sample was in the Wenzel-Cassie state at this point.

3.4 Capillary water absorption analysis

Figure 8 illustrates the relationship between the capillary water absorption rate of hydrophobic modified cement-based materials prepared with different sandpaper grit sizes and time, with 0 representing the untreated cement block as the control group. The graph indicates that the materials prepared with 400 grit sandpaper exhibit the lowest capillary water absorption at saturation, followed by 1,200 grit and 2000, then 800 grit, while those prepared with 120 and 220 grit show higher capillary water absorption. This is consistent with the previously observed wetting behavior. At this point, the microstructure construction has reduced the capillary water absorption by 90.63% compared to the control group.

Moreover, the hydrophobic surface delays the onset of the rapid water absorption region. This is attributed to the Wenzel state of the hydrophobic surface, where repulsive forces exist between the hydrophobic groups on the sample surface and water molecules. Water must overcome these surface forces to be absorbed by the sample's capillaries, and at this point, the rate of capillary water absorption is controlled by the strength of the sample's surface hydrophobicity. From the previous analysis, it is evident that from 400 grit onwards, a high level of roughness can be achieved in the hydrophobic cement-based materials, as shown in Figure 1. The wettability results indicate minimal differences in surface wetting properties for samples prepared with grits above 400. According to our new definition of surface roughness, the roughness values are 1.2372 for 400 grit, 1.2376 for 800 grit, 1.2380 for 1,200 grit, and 1.2374 for 2000 grit samples. The original definition of

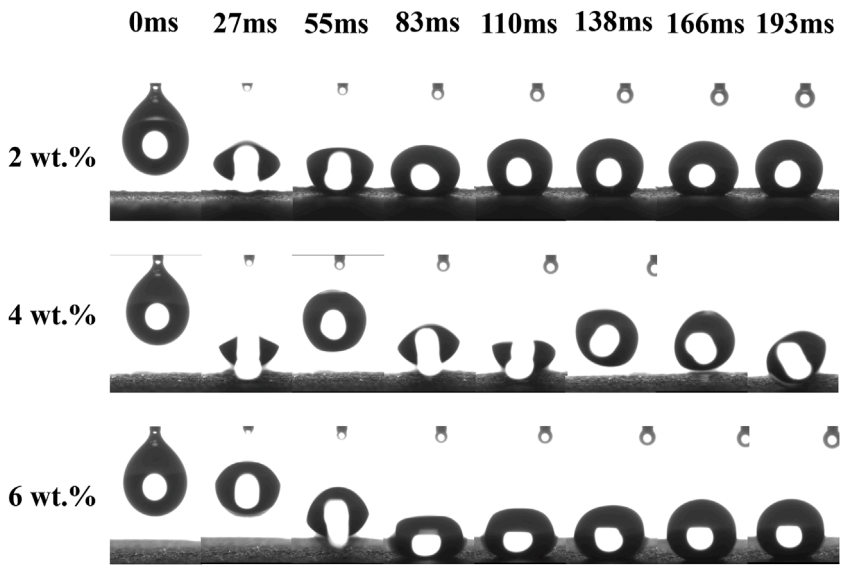

FIGURE 7
Bouncing behavior of the sample surface at 2 wt%, 4 wt%, and 6 wt% of nano-SiO_2.

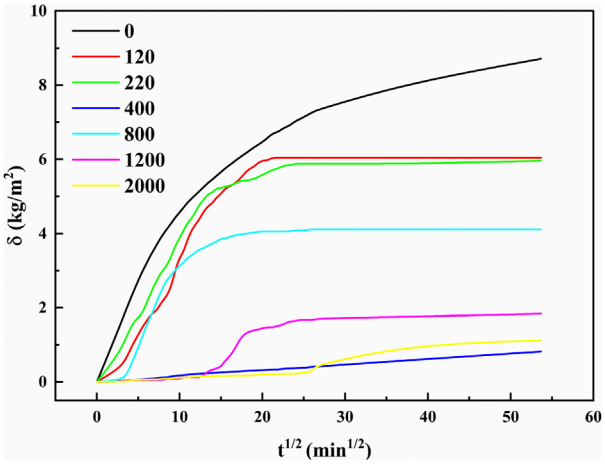

FIGURE 8
Capillary water absorption of hydrophobically modified cement-based materials prepared with different grits of sandpaper.

roughness is the ratio of the actual surface area to the projected surface area. The projected area of all samples is 35 × 35 mm^2, and calculations reveal that the actual surface area of the 400 grit sample is relatively low. The hydrophobic performance of the 800 grit sample is weaker compared to the 400, 1,200, and 2000 grit samples, resulting in higher water absorption. The 1,200 grit sample has a larger actual surface area, providing more sites for water penetration, thus absorbing more water compared to the 400 and 2000 grit samples. The smaller surface area of the 400 grit sample causes it to reach the rapid water absorption region more quickly. During the rapid water absorption phase, the similarity in the slope of the curves indicates a negligible difference in the rate of water absorption. This suggests that the micro-nano hierarchical structure of the prepared hydrophobic cementitious material merely impedes the entry of water but does not hinder the water's rapid transmission within the material's interior.

Figure 9 presents the functional relationship between the capillary water absorption rate of hydrophobic modified cement-based materials prepared with varying dosages of nano-SiO_2 and time, with 0 representing the untreated cement block as the control group. The circles in Figure 9 represent the onset of the rapid water absorption region for each sample. The data indicates that the samples prepared with 4 wt% nano-SiO_2 exhibited the lowest capillary water uptake, while those with 6 wt% and 8 wt% showed negligible differences. Samples without nano-SiO_2 and those with 2 wt% had higher capillary water absorption, with the nanostructure construction achieving a maximum reduction in total capillary water absorption of 94.37% compared to the control group. Similarly, the hydrophobic surface delayed the onset of the rapid water absorption region, as indicated by the circles in Figure 9. The rapid water absorption onset times, from fastest to slowest, are as follows: 0 wt%, 2 wt%, 6 wt%, 8 wt%, and 4 wt%. This delay is likely due to the Wenzel-Cassie and Cassie states of the hydrophobic surface. In these states, water does not fully contact the rough surface but is separated by trapped air between the liquid and solid. Before the liquid can contact the rough surface, it must displace the air, with the controlling factor for the rate of capillary water absorption being the air pressure retained by the hydrophobic surface (Yang et al., 2021). This results in no significant change in mass during the early stages of capillary water absorption. For hydrophobic cement-based materials with a pronounced delay in water absorption, higher contact angle values imply a more positive effect on delaying water absorption. The performance of hydrophobic modified cement-based materials prepared with different dosages of nano-SiO_2 in the rapid water absorption region was similar in terms of the rate of capillary water absorption, yet there were differences in the final total capillary absorption.

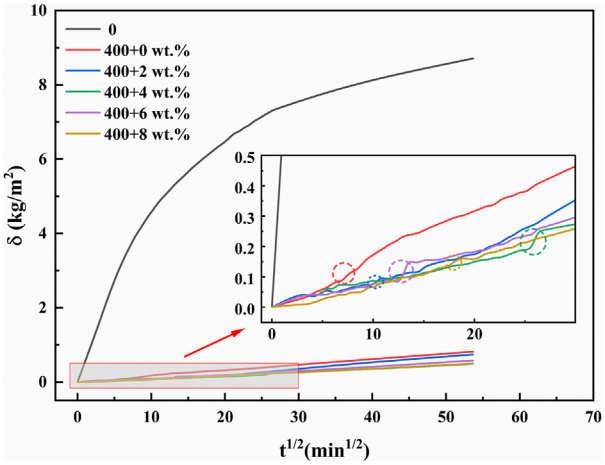

FIGURE 9
Capillary water absorption of hydrophobic cement-based materials prepared by spraying PDMS with different nano-SiO_2 contents. Circles: the onset of the rapid water absorption region.

3.5 Stability of hydrophobic properties

Cement-based materials are prone to damage. Their hydrophobic performance is limited by the surface structure. Therefore, the mechanical strength of the hydrophobic structure is an important factor (Wang et al., 2020b). It affects its application in practical engineering. Currently, there is an absence of an adequate apparatus or methodology to assess the mechanical stability of superhydrophobic materials. The stability of superhydrophobic materials can be assessed through manual means. The stability of superhydrophobic materials is evaluated through the measurement of alterations in their WCA and SA following the application of diverse mechanical damages, including sandpaper polishing, double-sided tape bonding and peeling, gravel impact, and knife cutting. Of the aforementioned methods, sandpaper polishing is the most frequently employed approach for assessing the mechanical stability of superhydrophobic surfaces in the scientific literature. This is because certain crucial experimental parameters, including pressure, sandpaper roughness, and the polishing distance (or number of times), can be readily regulated. In this study, the mechanical stability of hydrophobic cement-based materials was evaluated through the use of sandpaper polishing and knife-cutting techniques.

The abrasion resistance characterization method of hydrophobic cement-based materials is shown in Figure 10. By the established characterization methodology, the abrasion resistance of hydrophobic cement-based materials was evaluated. First, the superhydrophobic surface of the hydrophobic cement-based material, which has been loaded with a 100 g weight, is brought into contact with a working surface of 800 grit sandpaper. Subsequently, the sample was displaced horizontally by 100 mm. It was then rotated by 90° and displaced horizontally once more by 100 mm. Following the abrasion test, the contact angle of the hydrophobic surface was gauged. Each 200 mm displacement is regarded as a cycle. The aforementioned cycle was repeated 50 times.

Figure 11 shows that the hydrophobic cement-based material with a surface contact angle of 151.5° still maintained superhydrophobic performance after 10 polishing cycles under a 100 g weight. In the early stage of abrasion, the surface contact angle slightly increased. This might be because the micro-nano hierarchical structure of the hydrophobic surface was not seriously damaged, and the abrasion increased the surface roughness. According to the Wenzel model, the wetting characteristics of the material surface are enhanced with the increase in roughness. The hydrophobic surface exhibits an increase in hydrophobicity, while the hydrophilic surface displays a corresponding increase in hydrophilicity. This results in an elevated surface contact angle for the sample. With the increase of polishing cycles, the contact angle of the cement-based material surface rapidly decreased, and the hydrophobic cement-based material surface lost its superhydrophobicity. In the 10–20 cycles, the surface contact angle was in a rapid decline stage, decreasing from 151.5° to 134.3°. In the 20–50 cycles, the surface contact angle of the sample slightly decreased, decreasing from 134.3° to 124.3°. This was because the nanostructure of the sample surface was continuously broken with the increase of abrasion cycles, and the micro-nano hierarchical structure gradually disappeared. Combined with Figure 8, it can be seen that the nanostructure was almost destroyed at about the 19th cycle. At this time, the micron structure and the low surface energy material PDMS synergized, making the surface contact angle change relatively stable. When the abrasion times reached 50, the hydrophobic surface showed obvious abrasion. However, even in the 50 abrasion cycles, it could maintain a surface contact angle above 120°, keeping the hydrophobic characteristics. This indicates that the hydrophobic cement-based material prepared in this paper has good mechanical stability.

To test the durability of the hydrophobic surface, we performed a knife-cutting experiment, which simulated the damage caused by sharp objects (Jiang et al., 2023). The coated surface was scraped repeatedly with a metal knife along orthogonal directions. After scraping the surface with a metal knife, we dropped water droplets on it and measured the contact angle. As shown in Figure 12A. The results are shown in Figure 12B. Despite the severe damage caused to the original hydrophobic surface by scraping, the surface did not peel off. Moreover, the water droplets remained spherical on the surface, and the WCA decreased slightly, but retained a value of approximately 150°, suggesting that the hydrophobic surface exhibited high mechanical stability. Figure 12C shows the water droplet sliding experiment. It can be seen that the surface was severely damaged by the metal knife, but the rolling of the water droplets was not significantly affected. The water droplets could easily roll off the sample surface.

According to previous studies, UV can induce a crosslinking reaction of PDMS, increasing its hardness and strength (Yu et al., 2023). However, UV can cause oxidation and cracking of PDMS, destroying the C-H and C-O bonds on the PDMS surface. This introduces hydrophilic groups, such as -OH, -COOH, *etc.* The surface properties of PDMS are changed, making it from hydrophobic to hydrophilic, increasing its surface energy and adhesion (Efimenko et al., 2002). Meanwhile, UV can also promote the formation of a glass-like SiO_x thin layer on the PDMS surface, preventing the hydrophobicity of the PDMS surface from recovering over time. Considering that cement-based materials will

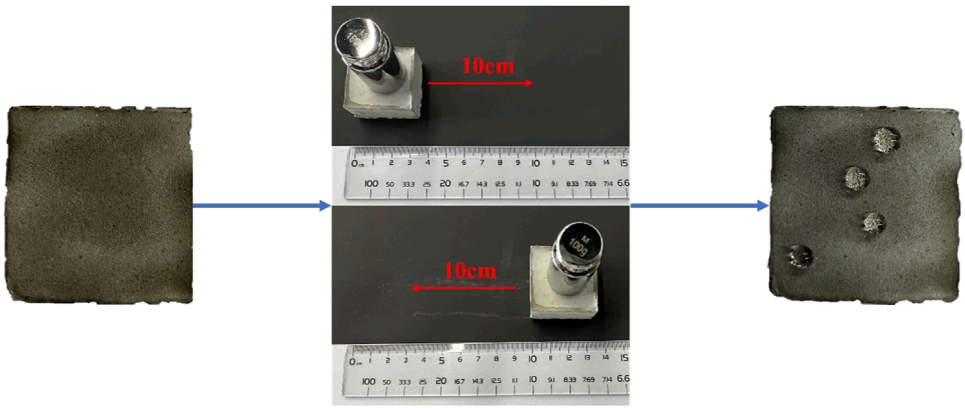

FIGURE 10
Abrasion test on hydrophobic cementitious materials.

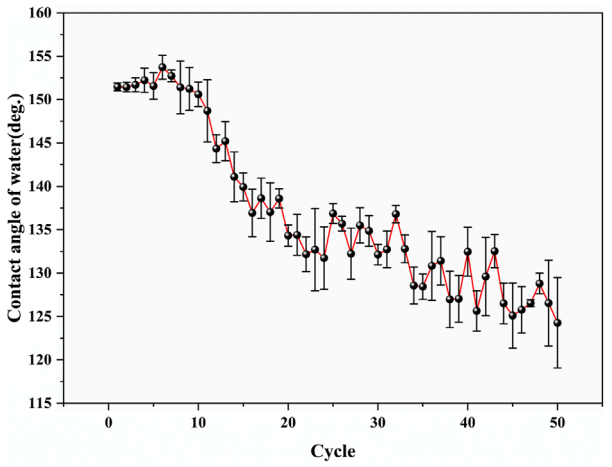

FIGURE 11
Surface contact angle after sandpaper abrasion.

constantly face light exposure during use, to evaluate the anti-ultraviolet aging performance of PDMS, the hydrophobic cement-based materials were subjected to an ultraviolet light exposure experiment. The FTIR spectra before and after UV irradiation of the hydrophobic cement-based material, the cement matrix and the PDMS are shown in Figure 13. The analysis of the infrared absorption spectrum of PDMS reveals that the absorption peak observed at approximately 2,963.09 cm^{-1} is attributed to the asymmetric C-H stretching vibration of the CH_3 group. The observed peak at 1,259.74 cm^{-1} is indicative of a symmetric deformation vibration of the Si-CH_3 group. The absorption peak observed at approximately 1,010.86 cm^{-1} can be attributed to the asymmetrical stretch vibration of the Si-O-Si bond present within the PDMS molecule. The absorption peak located at 794.76 cm^{-1} has been identified as resulting from the vibrational motion of the Si-$(CH_3)_2$ group. These absorption peaks are typical characteristic peaks of PDMS (Tang et al., 2023). In addition, in contrast to the typical spectral features of PDMS, an evident absorption peak was discerned at 1,402 and 870 cm^{-1} for hydrophobic cement-based materials. This correlates with the chemical absorption peak of the C-S-H gel. The hydrophobic samples and PDMS have absorption peaks near 794, 1,010, 1,259, and 2,963 cm^{-1}, indicating that PDMS was successfully introduced into the hydrophobic cement-based materials. Compared with PDMS, the Si-O-Si bond in the hydrophobic cement-based materials moved from 1,010.86 cm^{-1} to 1,014.37 cm^{-1}, which means an increase in Si-O. This also indicates that the PDMS molecule chemically bonded with the surface of the cement hydration product (C-S-H). According to Stewart (Stewart et al., 2013), the incorporation of PDMS has been observed to enhance the bridging oxygen levels within the C-S-H structure. Furthermore, research by Zhu and colleagues has indicated that PDMS can establish covalent linkages with C-S-H, thereby serving a pivotal bridging function (Zhu et al., 2021). After 24 h of ultraviolet irradiation, the hydrophobic performance of the sample surface slightly decreased, and the surface WCA decreased from 151.5° to 151°. Subsequently, the surface WCA had a slight recovery after 24 h of avoiding light, as shown in Figure 14. After 24 h of ultraviolet irradiation, the characteristic absorption peaks of PDMS were still strong, and the wetting property of the sample surface hardly changed, indicating that the hydrophobic surface had high photothermal stability.

In the study of the hydrophobic durability of cement-based materials, simulating rainwater impact is a crucial experimental step. In this experiment, the cementitious material was inclined at 28° to mimic the flow of rainwater on a slope. Tap water fell from a height of 10 cm at a rate of 8 drops per second, continuously impacting the material's surface for 30 min. After the impact, the surface water was absorbed using blotting paper. Subsequently, the hydrophobicity of the material surface was assessed by measuring the WCA. The experiment also included a thermal treatment step, where the material was dried in an oven at 40°C for 30 min to simulate the natural drying process. From the start of the water impact to the end of the thermal treatment constituted a complete cycle, and this study conducted ten such cycles.

The experimental results, as shown in Figure 15, showed that after the water impact, the WCA decreased from the initial 154.6°–152.9°, indicating a reduction in surface hydrophobicity.

10.3389/fmats.2024.1512374

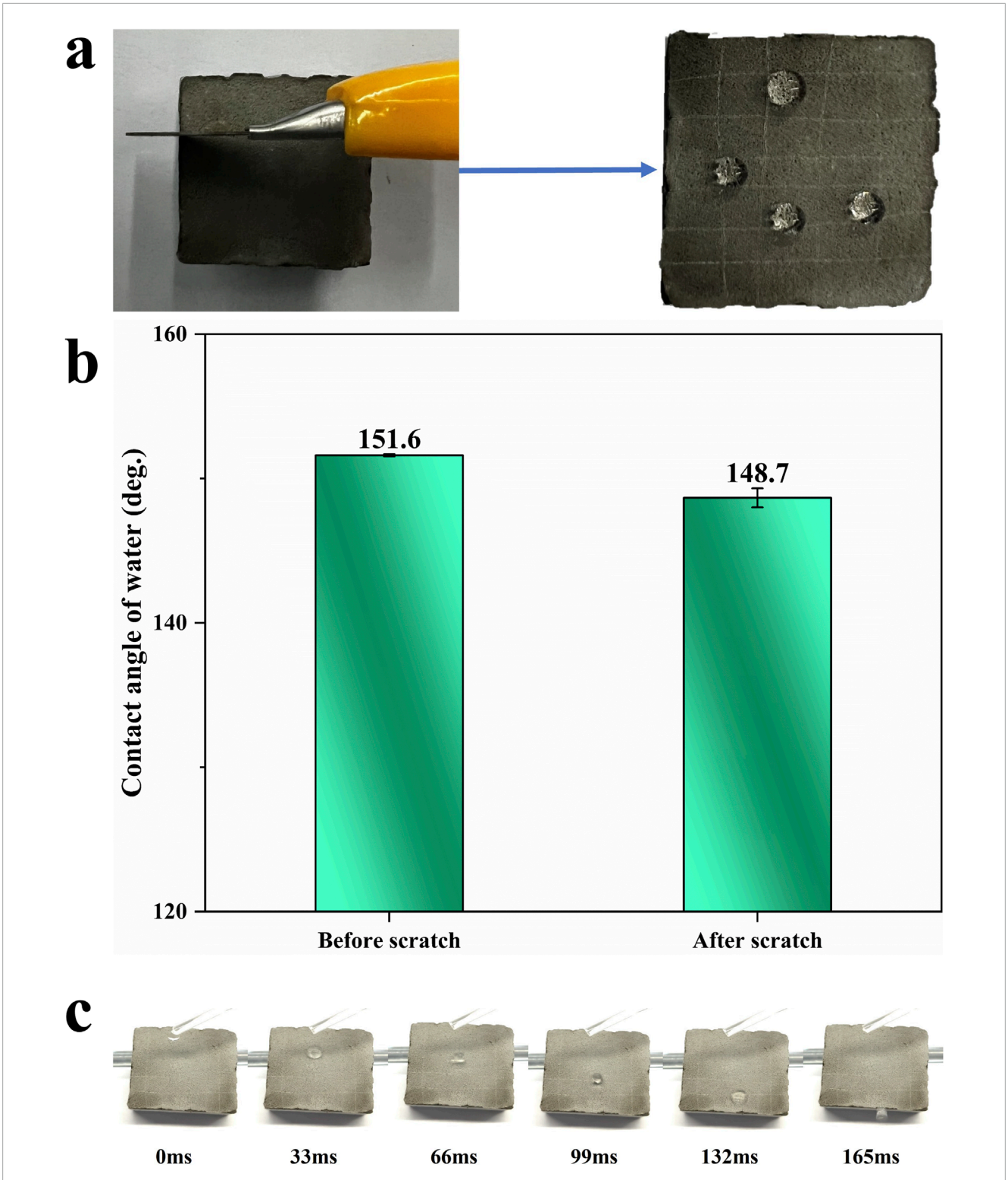

FIGURE 12
(A) Schematic diagram of knife scratching experiment; **(B)** Wettability of hydrophobic surfaces of samples before and after scratching; **(C)** Experiment of water droplet slipping after knife scratching.

However, after thermal treatment, the WCA recovered to 154.3°, close to its original state. This recovery phenomenon was also observed in subsequent cycles, with the WCA stabilizing around 145° from the fifth cycle onwards. The decrease in WCA was mainly attributed to microstructural damage caused by the water impact and the loss of low-surface-energy substances, manifested as the shedding of surface nanoparticles and partial peeling of the PDMS layer. The recovery of the WCA was due to the

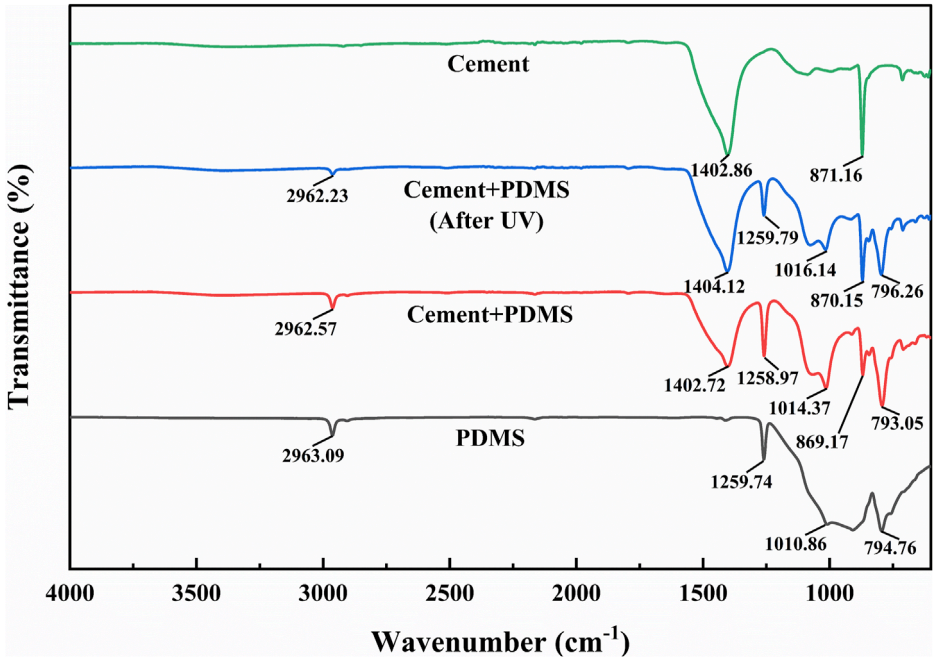

FIGURE 13
FTIR spectra of the hydrophobic surface of the sample before and after UV irradiation.

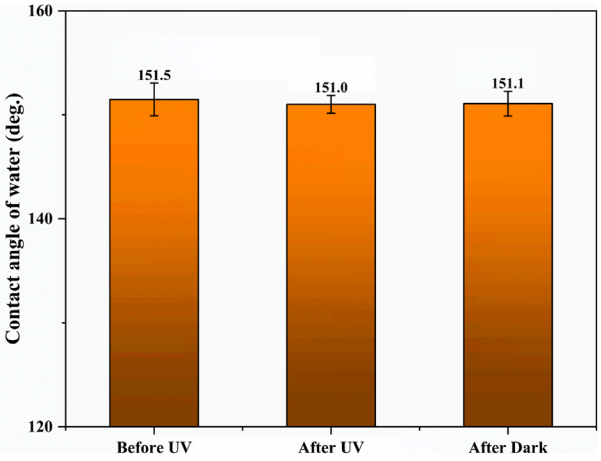

FIGURE 14
Effect of UV irradiation and darkness on the surface wettability of samples.

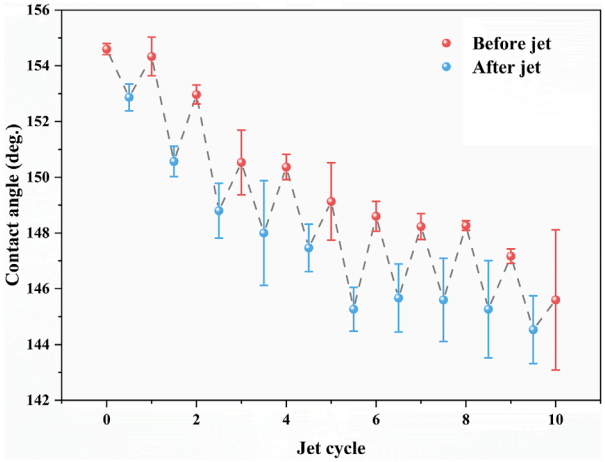

FIGURE 15
Effect of the water impact on WCA of the hydrophobic surface of the sample.

thermal treatment promoting the migration of PDMS molecules from the interior to the surface of the material, replenishing the surface PDMS, thereby compensating for the lost low-surface-energy substances (Long et al., 2017). The gradual decrease in WCA after recovery could be attributed to the irreversible shedding of nanoparticles. As the number of impact cycles increased, the continuous reduction of nanoparticles led to the gradual disappearance of the micro-nanostructure on the sample surface. This process increased the adhesion of water droplets on the sample surface, further reducing the WCA.

4 Conclusion

Our study demonstrates the feasibility and potential of cement-based materials with hierarchical structures and superhydrophobic properties for practical applications. By precisely controlling the surface roughness, we achieved superhydrophobicity with a WCA of 155.7° and reduced water absorption by 94.37%. The materials exhibited remarkable hydrophobic performance, maintaining a WCA above 120° even after mechanical damage, thermal erosion,

and water impact tests. These findings underscore the material's capability to enhance the durability and waterproofing of building structures, contributing to the development of sustainable and impermeable construction materials. They provide valuable insights into the advancement of durable hydrophobic materials in the construction industry.

Data availability statement

The original contributions presented in the study are included in the article/supplementary material, further inquiries can be directed to the corresponding author.

Author contributions

XB: Investigation, Writing–original draft. WY: Funding acquisition, Supervision, Writing–review and editing. GaL: Investigation, Supervision, Writing–review and editing. GuL: Investigation, Supervision, Writing–review and editing. AS: Investigation, Supervision, Writing–review and editing. YW: Investigation, Supervision, Writing–review and editing.

Funding

The author(s) declare that financial support was received for the research, authorship, and/or publication of this article. National Key Research and Development Program of China (Project No. 2019YFC1906203).

Acknowledgments

The authors gratefully acknowledge the financial support provided by the National Key Research and Development Program of China (Project No. 2019YFC1906203).

Conflict of interest

The authors declare that the research was conducted in the absence of any commercial or financial relationships that could be construed as a potential conflict of interest.

Generative AI statement

The author(s) declare that no Generative AI was used in the creation of this manuscript.

Publisher's note

All claims expressed in this article are solely those of the authors and do not necessarily represent those of their affiliated organizations, or those of the publisher, the editors and the reviewers. Any product that may be evaluated in this article, or claim that may be made by its manufacturer, is not guaranteed or endorsed by the publisher.

References

Ammar, S. H., Ramesh, K., Ma, I. A. W., Farah, Z., Vengadaesvaran, B., Ramesh, S., et al. (2017). Studies on SiO_2-hybrid polymeric nanocomposite coatings with superior corrosion protection and hydrophobicity. *Surf. Coat. Technol.* 324, 536–545. doi:10.1016/j.surfcoat.2017.06.014

Cao, Y., Wang, Q., Zhou, W., Chang, X., Wang, Y., and Gong, X. (2024). Fabrication of hierarchical superhydrophobic structures by silane enriched with nanomaterials for enhancing permeability and freeze-thaw resistance. *Constr. Build. Mat.* 426, 136016. doi:10.1016/j.conbuildmat.2024.136016

Cassie, A. B. D., and Baxter, S. (1944). Wettability of porous surfaces. *Trans. Faraday Soc.* 40, 546. doi:10.1039/tf9444000546

Chen, H., Zuo, Z., Tian, Q., Xue, S., Qiu, F., Peng, X., et al. (2023a). Waste to treasure: A superwetting fiber membrane from waste PET plastic for water-in-oil emulsion separation. *J. Clean. Prod.* 396, 136502. doi:10.1016/j.jclepro.2023.136502

Chen, K., Li, Y., Yang, G., Hu, S., Shi, Z., and Yang, G. (2023b). Fabric-based TENG woven with bio-fabricated superhydrophobic bacterial cellulose fiber for energy harvesting and motion detection. *Adv. Funct. Mat.* 33, 2304809. doi:10.1002/adfm.202304809

Chen, Z., Lu, Y., Li, R., Li, D., Xiang, B., Li, J., et al. (2023c). Liquid-solid contact electrification through the lens of surface and interface science. *Nano Energy* 116, 108834. doi:10.1016/j.nanoen.2023.108834

Efimenko, K., Wallace, W. E., and Genzer, J. (2002). Surface modification of sylgard-184 poly(dimethyl siloxane) networks by ultraviolet and ultraviolet/ozone treatment. *J. Colloid Interface Sci.* 254, 306–315. doi:10.1006/jcis.2002.8594

Gao, Y., Wang, F., Liu, P., Zhang, W., and Yang, L. (2019). Superhydrophobic behavior of magnesium oxychloride cement surface with a dual-level fractal structure. *Constr. Build. Mat.* 210, 132–139. doi:10.1016/j.conbuildmat.2019.03.158

Han, K., Yin, B., Jia, X., Xu, H., Li, T., Wang, P., et al. (2024). One-step hybridization of silane hydrolysis and silica mineralization for enhanced superhydrophobic coating on cement-based materials. *J. Build. Eng.* 94, 109824. doi:10.1016/j.jobe.2024.109824

He, S., Chen, J., Lu, Y., Huang, S., and Feng, K. (2024). Enhanced waterproof performance of superhydrophobic SiO_2/PDMS coating. *Prog. Org. Coat.* 197, 108845. doi:10.1016/j.porgcoat.2024.108845

Heo, K. J., Yoo, J. H., Shin, J., Huang, W., Tiwari, M. K., Jung, J. H., et al. (2024). Transition from the Wenzel to Cassie–Baxter state by PFOTES/TiO_2 nanoparticles leading to a mechanically robust and damage/contamination-recoverable surface. *J. Mat. Chem.a* 12, 3886–3895. doi:10.1039/D3TA06521A

Indumathy, B., Sathiyanathan, P., Prasad, G., Reza, M. S., Prabu, A. A., and Kim, H. (2023). A comprehensive review on processing, development and applications of organofunctional silanes and silane-based hyperbranched polymers. *Polymers* 15, 2517. doi:10.3390/polym15112517

Jiang, L. (2003). Nanostructured materials with superhydrophobic surface-from nature to biomimesis. *Chem. Industry Eng. Prog.*, 22(12):1258–1264.

Jiang, L., Zheng, H., Xiong, J., Fan, Z., Shen, T., Xie, H., et al. (2023). Fabrication of negative carbon superhydrophobic self-cleaning concrete coating: high added-value utilization of recycled powders. *Cem. Concr. Compos.* 136, 104882. doi:10.1016/j.cemconcomp.2022.104882

Lan, L., Di, Y., Wang, H., Huang, Y., Zhu, L., and Li, X. (2023). One-step modification method of a superhydrophobic surface for excellent antibacterial capability. *Friction* 11, 524–537. doi:10.1007/s40544-022-0611-z

Lange, D. A., Jennings, H. M., and Shah, S. P. (1993). Relationship between fracture surface roughness and fracture behavior of cement paste and mortar. *J. Am. Ceram. Soc.* 76, 589–597. doi:10.1111/j.1151-2916.1993.tb03646.x

Li, K., Wang, Y., Wang, X., Zhang, X., Zhang, J., Xie, H., et al. (2021). Superhydrophobic magnesium oxychloride cement based composites with integral stability and recyclability. *Cem. Concr. Compos.* 118, 103973. doi:10.1016/j.cemconcomp.2021.103973

Li, Y., Li, L., Wan, D., Sha, A., Li, Y., and Liu, Z. (2022). Preparation and evaluation of a fluorinated nano-silica superhydrophobic coating for cement pavement. *Constr. Build. Mat.* 360, 129478. doi:10.1016/j.conbuildmat.2022.129478

Liang, C., Zhao, P., Liu, L., Wang, S., Wang, S., Sobolev, K., et al. (2023). Fabrication of bulk hydrophobic cement-based materials with ultra-high impermeability. *J. Build. Eng.* 63, 105492. doi:10.1016/j.jobe.2022.105492

Liao, G., Yao, W., She, A., and Bian, X. (2023a). An eco-friendly building coating with high self-cleaning capacity: synergetic effect of super-hydrophobicity and photocatalytic degradation. *Constr. Build. Mat.* 406, 133406. doi:10.1016/j.conbuildmat.2023.133406

Liao, G., Yao, W., She, A., Shi, C., Zuo, J., and Wu, D. (2023b). Interfacial design of nano-TiO2 modified recycled concrete powder for building self-cleaning. *Colloids Surf. A* 661, 130925. doi:10.1016/j.colsurfa.2023.130925

Liu, P., Gao, Y., Wang, F., Yang, J., Yu, X., Zhang, W., et al. (2017). Superhydrophobic and self-cleaning behavior of Portland cement with lotus-leaf-like microstructure. *J. Clean. Prod.* 156, 775–785. doi:10.1016/j.jclepro.2017.03.211

Long, M., Peng, S., Deng, W., Yang, X., Miao, K., Wen, N., et al. (2017). Robust and thermal-healing superhydrophobic surfaces by spin-coating of polydimethylsiloxane. *J. Colloid Interface Sci.* 508, 18–27. doi:10.1016/j.jcis.2017.08.027

Mao, Y., Huang, Q., Meng, B., Zhou, K., Liu, G., Gugliuzza, A., et al. (2020). Roughness-enhanced hydrophobic graphene oxide membrane for water desalination via membrane distillation. *J. Membr. Sci.* 611, 118364. doi:10.1016/j.memsci.2020.118364

Meng, X., Chen, Z., Qian, C., Song, Z., Wang, L., Li, Q., et al. (2023). Hierarchical superhydrophobic poly(vinylidene fluoride-*co*-hexafluoropropylene) membrane with a bead (SiO_2 nanoparticles)-on-string (nanofibers) structure for all-day passive radiative cooling. *ACS Appl. Mat. Interfaces* 15, 2256–2266. doi:10.1021/acsami.2c19422

Muzenski, S., Flores-Vivian, I., and Sobolev, K. (2020). Hydrophobic modification of ultra-high-performance fiber-reinforced composites with matrices enhanced by aluminum oxide nano-fibers. *Constr. Build. Mat.* 244, 118354. doi:10.1016/j.conbuildmat.2020.118354

Nguyen, K. T. Q., Navaratnam, S., Mendis, P., Zhang, K., Barnett, J., and Wang, H. (2020). Fire safety of composites in prefabricated buildings: from fibre reinforced polymer to textile reinforced concrete. *Compos. Part B Eng.* 187, 107815. doi:10.1016/j.compositesb.2020.107815

Ni, X., Gao, Y., Zhang, X., Lei, Y., Sun, G., and You, B. (2021). An eco-friendly smart self-healing coating with NIR and pH dual-responsive superhydrophobic properties based on biomimetic stimuli-responsive mesoporous polydopamine microspheres. *Chem. Eng. J.* 406, 126725. doi:10.1016/j.cej.2020.126725

Packham, D. E. (2003). Surface energy, surface topography and adhesion. *Int. J. Adhes. Adhes.* 23, 437–448. doi:10.1016/S0143-7496(03)00068-X

Palacios, M., Sanz-Pont, D., Kunhi Mohamed, A., Boscaro, F., Reiter, L., Marchon, D., et al. (2022). Heating cement to slow down its hydration: the unexpected role of PCE interpolymer bridge formation. *Cem. Concr. Res.* 156, 106765. doi:10.1016/j.cemconres.2022.106765

Schutzius, T. M., Jung, S., Maitra, T., Graeber, G., Köhme, M., and Poulikakos, D. (2015). Spontaneous droplet trampolining on rigid superhydrophobic surfaces. *Nature* 527, 82–85. doi:10.1038/nature15738

She, W., Zheng, Z., Zhang, Q., Zuo, W., Yang, J., Zhang, Y., et al. (2020). Predesigning matrix-directed super-hydrophobization and hierarchical strengthening of cement foam. *Cem. Concr. Res.* 131, 106029. doi:10.1016/j.cemconres.2020.106029

Shen, Y., Li, K., Chen, H., Wu, Z., and Wang, Z. (2021). Superhydrophobic F-SiO_2@PDMS composite coatings prepared by a two-step spraying method for the interface erosion mechanism and anti-corrosive applications. *Chem. Eng. J.* 413, 127455. doi:10.1016/j.cej.2020.127455

Shi, S., Wang, X., Li, Z., Meng, J., Chu, X., Zhang, P., et al. (2023). Multifunctional integrated superhydrophobic coatings with unique fluorescence and micro/micro/nano-hierarchical structures enabled by *in situ* self-assembly. *ACS Appl. Mat. Interfaces* 15, 7442–7453. doi:10.1021/acsami.2c21531

Sow, P. K., Singhal, R., Sahoo, P., and Radhakanth, S. (2021). Fabricating low-cost, robust superhydrophobic coatings with re-entrant topology for self-cleaning, corrosion inhibition, and oil-water separation. *J. Colloid Interface Sci.* 600, 358–372. doi:10.1016/j.jcis.2021.05.026

Stewart, A., Schlosser, B., and Douglas, E. P. (2013). Surface modification of cured cement pastes by silane coupling agents. *ACS Appl. Mat. Interfaces* 5, 1218–1225. doi:10.1021/am301967v

Su, C., Huang, X., Zhang, L., Zhang, Y., Yu, Z., Chen, C., et al. (2023). Robust superhydrophobic wearable piezoelectric nanogenerators for self-powered body motion sensors. *Nano Energy* 107, 108095. doi:10.1016/j.nanoen.2022.108095

Szafarska, M., Olszok, V., Holländer, U., Gustus, R., Weber, A. P., and Maus-Friedrichs, W. (2023). Gas phase reaction of silane with water at different temperatures and supported by plasma. *ACS Omega* 8, 8388–8396. doi:10.1021/acsomega.2c07209

Tang, D., Yang, C., Shen, C., Yu, L., Tian, Y., and Zhu, X. (2023). Preparing hydrophobic alkali-activated slag mortar with lotus-leaf-like microstructure by adding polydimethylsiloxane (PDMS). *Constr. Build. Mat.* 409, 134148. doi:10.1016/j.conbuildmat.2023.134148

Tao, J., Dong, L., Wu, Y., Liu, X., Xie, J., Wu, H., et al. (2024). Fabrication of room temperature self-healing, robust superhydrophobic coatings via spraying dual cross-linking supramolecular silicone polymer/SiO_2 composite. *Compos. Part B Eng.* 273, 111245. doi:10.1016/j.compositesb.2024.111245

Tonon, C. C., De Souza Rastelli, A. N., Bodahandi, C., Ghosh, G., Hasan, T., Xu, Q., et al. (2023). Superhydrophobic tipped antimicrobial photodynamic therapy device for the *in vivo* treatment of periodontitis using a wistar rat model. *ACS Appl. Mat. Interfaces* 15, 50083–50094. doi:10.1021/acsami.3c12820

Wang, F., Lei, S., Ou, J., and Li, W. (2020a). Effect of PDMS on the waterproofing performance and corrosion resistance of cement mortar. *Appl. Surf. Sci.* 507, 145016. doi:10.1016/j.apsusc.2019.145016

Wang, F., Liu, H., Ou, J., and Li, W. (2021a). Fast fabrication of superhydrophobic surfaces on hardened cement paste using sodium laurate aqueous solution. *Constr. Build. Mat.* 278, 122385. doi:10.1016/j.conbuildmat.2021.122385

Wang, F., Xie, T., Lei, S., Ou, J., Li, W., Xue, M., et al. (2020b). Preparation and properties of foundry dust/Portland cement based composites and superhydrophobic coatings. *Constr. Build. Mat.* 246, 118466. doi:10.1016/j.conbuildmat.2020.118466

Wang, N., Wang, Q., Xu, S., and Lei, L. (2021b). Fabrication of hierarchical structures on concrete surfaces with superhydrophobicity using replicated micro-nano dendritic structures. *J. Ind. Eng. Chem.* 103, 314–321. doi:10.1016/j.jiec.2021.07.047

Wang, P., Zeng, J., Yan, X., Tan, P., Wang, M., Zheng, Y., et al. (2023). A three-layer superhydrophobic coatings inspired by human scalp structure with excellent anti-reflection and durable effects for photovoltaic applications. *J. Clean. Prod.* 414, 137605. doi:10.1016/j.jclepro.2023.137605

Wang, R., Zhang, Q., and Li, Y. (2022). Deterioration of concrete under the coupling effects of freeze–thaw cycles and other actions: a review. *Constr. Build. Mat.* 319, 126045. doi:10.1016/j.conbuildmat.2021.126045

Wang, S., Liu, K., Yao, X., and Jiang, L. (2015). Bioinspired surfaces with superwettability: new insight on theory, design, and applications. *Chem. Rev.* 115, 8230–8293. doi:10.1021/cr400083y

Wang, W., Wang, S., Yao, D., Wang, X., Yu, X., and Zhang, Y. (2020c). Fabrication of all-dimensional superhydrophobic mortar with enhanced waterproof ability and freeze-thaw resistance. *Constr. Build. Mat.* 238, 117626. doi:10.1016/j.conbuildmat.2019.117626

Wenzel, R. N. (1936). Resistance of solid surfaces to wetting by water. *Ind. Eng. Chem.* 28, 988–994. doi:10.1021/ie50320a024

Wu, F., Yu, Q., and Chen, X. (2023a). Unleashing the potential of bio-based concrete: investigating its long-term mechanical strength and drying shrinkage in real climatic environments. *Cem. Concr. Compos.* 143, 105237. doi:10.1016/j.cemconcomp.2023.105237

Wu, Y., Dong, L., Shu, X., Yang, Y., She, W., and Ran, Q. (2022). A review on recent advances in the fabrication and evaluation of superhydrophobic concrete. *Compos. Part B Eng.* 237, 109867. doi:10.1016/j.compositesb.2022.109867

Wu, Y., Shu, X., Yang, Y., She, W., Dong, L., and Ran, Q. (2023b). Fabrication of robust and room-temperature curable superhydrophobic composite coatings with breathable and anti-icing performance. *Chem. Eng. J.* 463, 142444. doi:10.1016/j.cej.2023.142444

Xia, D., and Brueck, S. R. J. (2008). Strongly anisotropic wetting on one-dimensional nanopatterned surfaces. *Nano Lett.* 8, 2819–2824. doi:10.1021/nl801394w

Xu, J., Liu, Q., Guo, H., Wang, M., Li, Z., and Sun, G. (2022). Low melting point alloy modified cement paste with enhanced flexural strength, lower hydration temperature, and improved electrical properties. *Compos. Part B Eng.* 232, 109628. doi:10.1016/j.compositesb.2022.109628

Yang, J., She, W., Zuo, W., Lyu, K., and Zhang, Q. (2021). Rational application of nano-SiO_2 in cement paste incorporated with silane: counterbalancing and synergistic effects. *Cem. Concr. Compos.* 118, 103959. doi:10.1016/j.cemconcomp.2021.103959

Yu, J., Zhang, C., Kong, X., Pang, X., and Jiang, L. (2021). Influence of silane emulsion hydrophobic agent on concrete properties. *J. Chin. Ceram. Soc.* 49, 372–380. doi:10.14062/j.issn.0454-5648.20200303

Yu, Y., Chen, L., Weng, D., Hou, Y., Pang, Z., Zhan, Z., et al. (2022). Effect of doping SiO_2 nanoparticles and phenylmethyl silicone oil on the large-scale deicing property of PDMS coatings. *ACS Appl. Mat. Interfaces* 14, 48250–48261. doi:10.1021/acsami.2c13650

Yu, Y., Weng, D., Chen, L., and Wang, J. (2023). Effective large-scale deicing based on the interfacial toughness tuning of a UV-curable PDMS coating. *Mater. Today Phys.* 35, 101134. doi:10.1016/j.mtphys.2023.101134

Zhang, H., Liu, Y.-Q., Zhao, S., Huang, L., Wang, Z., Gao, Z., et al. (2023). Transparent and robust superhydrophobic structure on silica glass processed with microstereolithography printing. *ACS Appl. Mat. Interfaces* 15, 38132–38142. doi:10.1021/acsami.3c08125

Zhang, W., Zheng, Q., Ashour, A., and Han, B. (2020a). Self-healing cement concrete composites for resilient infrastructures: a review. *Compos. Part B Eng.* 189, 107892. doi:10.1016/j.compositesb.2020.107892

Zhang, X.-F., Chen, Y.-Q., and Hu, J.-M. (2020b). Robust superhydrophobic SiO_2/polydimethylsiloxane films coated on mild steel for corrosion protection. *Corros. Sci.* 166, 108452. doi:10.1016/j.corsci.2020.108452

Zhao, J., Gao, X., Chen, S., Lin, H., Li, Z., and Lin, X. (2022). Hydrophobic or superhydrophobic modification of cement-based materials: a systematic review. *Compos. Part B Eng.* 243, 110104. doi:10.1016/j.compositesb.2022.110104

Zhao, S., Ma, Z., Song, M., Tan, L., Zhao, H., and Ren, L. (2023). Golden section criterion to achieve droplet trampoline effect on metal-based superhydrophobic surface. *Nat. Commun.* 14, 6572. doi:10.1038/s41467-023-42375-3

Zhu, J., and Duan, Y. (2024). Facilely etching of superhydrophobic surface with regular mulriple hierarchical micro-nano structures for crowning wettability. *Appl. Surf. Sci.* 648, 159009. doi:10.1016/j.apsusc.2023.159009

Zhu, Z., Wang, Z., Zhou, Y., Wei, Y., and She, A. (2021). Synthesis and structure of calcium silicate hydrate (C-S-H) modified by hydroxyl-terminated polydimethylsiloxane (PDMS). *Constr. Build. Mat.* 267, 120731. doi:10.1016/j.conbuildmat.2020.120731